A Dual-Band Energy Harvesting System Based on Metamaterial Transmission Lines

Chaiyong Soemphol
Research Unit for Electrical and Computer Engineering Technology (RECENT), Faculty of Engineering, Mahasarakham University, Thailand
chaiyong.s@msu.ac.th

Amornthep Sonsilphong
Department of Automation Robotic and Intelligent System Engineering, Faculty of Engineering, Khonkaen University, Thailand
amornso@kku.ac.th (corresponding author)

Received: 8 May 2025 | Revised: 15 July 2025 and 3 August 2025 | Accepted: 9 August 2025

 DOI: https://doi.org/10.48084/etasr.11998

ABSTRACT

The growth of wireless communication systems and the proliferation of Internet of Things (IoT) devices have spurred significant interest in the development of energy harvesting techniques to power these devices autonomously. Radio Frequency (RF) energy harvesting, utilizing electromagnetic waves as a power source, has emerged as a promising solution due to its ubiquity and availability. This paper presents the design, simulation, and experimental validation of a metamaterial-based rectenna system for efficient RF energy harvesting, specifically designed for Wi-Fi frequencies of 2.4 and 5.0 GHz. The experimental results show that the obtained reflection coefficient (S_{11}) confirms the impedance matching and resonance behavior, showing good agreement between the simulated and measured results. The rectifier's output voltage and RF-to-DC conversion efficiency were evaluated across various input power levels and frequencies, achieving a peak efficiency of approximately 72% at 5 dBm. Moreover, the load sensitivity analysis revealed a stable operation across a broad range of resistances, whereas the distance-dependent measurements confirmed the rectenna's capability to maintain a measurable output up to 250 cm from the source. These results validate that the proposed metamaterial transmission line can be used as an impedance matching part for low-power wireless energy harvesting applications.

Keywords-RF energy harvesting; metamaterial; transmission line; wi-fi signal; impedance matching

I. INTRODUCTION

Wireless energy harvesting is an innovative technology with the potential to power low-energy systems, such as wireless communication devices and sensor networks, without the need for traditional wiring [1]. Wireless energy harvesting harnesses unused energy from the surrounding environment, making it a promising solution for reducing the environmental impact, particularly in battery-free low-power sensors. However, the energy levels currently harvested from ambient sources remain insufficient to reliably power the low-energy devices. Hence, researchers have developed numerous designs to enhance the energy collection from various sources, such as Wi-Fi access points [2, 3], cellular base stations [4], radio broadcast stations (FM/AM radio) [5], and television/digital television (TV/DTV) [6]. It has been reported that a critical component in wireless energy harvesting systems is the microwave rectifier, which converts the received microwave signals into usable DC power. The efficiency of this conversion process is crucial for the overall performance of the system. Several single-band rectifiers have been developed for energy harvesting applications [7, 8]. However, to optimize the amount of harvested energy, a multi-frequency or broadband approach has proven to be more effective, allowing for greater exploitation of the available ambient RF energy harvesting systems [9-11]. Multiband rectifiers can capture energy across multiple frequency ranges, resulting in a higher DC output. As a result, these multiband designs have garnered significant interest. The design of multiband rectifiers hinges on the input-matching network, which ensures a maximum power transfer. Various network configurations have been explored, including single-stage T-type networks [12], two-stage T-type networks [13], multi-stub networks [14, 15], coupled lines [16], and LC networks [17, 18]. In addition, the use of metamaterials in energy harvesting systems has been investigated.

Electromagnetic metamaterials, which are artificially engineered structures with periodic metallic resonators, exhibit unique properties not found in nature, such as a negative refractive index [19] or zero refractive index [20]. In RF energy harvesting applications, metamaterials offer significant potential by improving the coupling between the incident electromagnetic waves and the harvesting device, thus increasing the energy capture efficiency. Additionally, the

ability of metamaterials to exhibit frequency selectivity allows targeted harvesting from specific frequency bands. The flexibility to control the electric permittivity (ϵ) and magnetic permeability (μ) of metamaterials enables more effective impedance matching between the antennas and their environment.

Impedance matching is a key application of metamaterials, offering the possibility of multiband matching through metamaterial transmission lines. Unlike traditional transmission lines, metamaterials provide greater flexibility by enabling the independent control of inductance (L) and capacitance (C), which can be adjusted by modifying the stub length, width, and coupling distance. The theoretical feasibility of multiband impedance matching using extended composite right/left-handed transmission lines was demonstrated in [21]. Practical implementations include impedance-matching structures, like Electromagnetic Band Gab (EBG) microstrip lines [22] and dual-band systems utilizing Split Ring Resonators (SRRs) [23]. Although SRRs reduced size, they may negatively affect the quality factor and complicate the design, as the relationship between the physical dimensions and electrical parameters is often unclear. Advancements have highlighted the potential of metasurfaces for impedance matching and proposed optimization techniques using composite right/left-handed transmission lines, which are particularly beneficial for RF energy-harvesting applications [24, 25].

The current study aims to address the challenge of efficiently harvesting energy from dual-band Wi-Fi signals using metamaterial transmission lines as part of multi-frequency impedance matching networks. An overview of the metamaterials is provided and the design and fabrication of the metamaterial transmission line are outlined, with a focus on the simulation and measurement results of the proposed structure. The measurement results are presented and the performance of the rectifier and rectenna systems is demonstrated. Furthermore, the practical implications and potential applications of the metamaterial-based RF energy-harvesting systems are discussed. Finally, the key contributions and findings of this study are summarized.

II. DESIGN AND FABRICATION OF METAMATERIAL TRANSMISSION LINE FOR RF ENERGY HARVESTING

The primary purpose of an RF energy harvesting system is to transform the RF power into usable electrical energy for low power devices. Figure 1 demonstrates such a system, designed for harvesting energy from ambient RF signals. The process begins with an antenna that captures the RF energy, which is then passed through an impedance matching network to optimize the power transfer to the rectification stage, typically diodes are used to convert the alternating RF signal into DC. Following this, a DC-pass filter removes the residual AC components, delivering a stable DC output suitable for powering low power electronic loads or storing energy. This work focuses on the impedance matching circuit part using a metamaterial-based transmission line. This specialized transmission medium enhances the signal handling before it is directed to the rectifier.

Metamaterials are artificially engineered materials with unique electromagnetic properties that arise from their subwavelength unit cells. These materials can manipulate the propagation of electromagnetic waves in ways that are unattainable with naturally occurring materials. Moreover, the ability of metamaterials to exhibit frequency selectivity offers the advantage of targeted energy harvesting from specific frequency bands. As stated above, metamaterial structures offer independent control over inductance (L) and capacitance (C), which can be precisely tuned by adjusting parameters, such as stub length, stub width, and the spacing between adjacent stubs. This added design flexibility introduces additional degrees of freedom, enabling effective impedance matching across the multiple frequency bands [24].

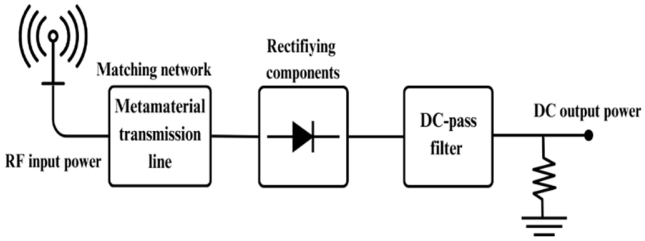

Fig. 1. The architecture of the proposed RF energy harvesting system.

Figure 2 illustrates the proposed metamaterial transmission line for energy harvesting. The design process for the proposed structure begins with defining the microstrip stub length (l) to achieve the first two half-wavelength ($\lambda/2$) resonances at 2.4 GHz and 5.0 GHz. A low-cost, 0.8 mm thick double copper-clad FR4 board was used as the substrate for all the simulations. This board has a dielectric constant (ε_r) of 4.3 and a dielectric loss tangent of 0.025. The design of the multi-input matching network is influenced by four key parameters: stub length, stub width, the spacing between adjacent stubs, and the gap between the input microstrip port and the stubs. The central frequencies of the operating bands are primarily determined by the stub length, which governs the $\lambda/2$ resonant frequency. The optimization process then focuses on fine-tuning both the stub length and the gap between the microstrip ports to minimize the reflection coefficient (S_{11}) at the first two $\lambda/2$ resonant frequencies, ensuring efficient energy harvesting performance across the targeted frequency bands.

The simulation results were generated using the CST Microwave Studio, employing a finite integration technique to evaluate the performance of the proposed metamaterial transmission line. The layout of the proposed structure is presented in Figure 2 (a) and the optimized dimensions of the metamaterial transmission line are: the overall width of the structure (W) is 39.00 mm, the width of the transmission line (W_t) is 1.00 mm, the width of the stubs (W_{s1}) is 1.65 mm, the width of the narrow sections (W_{s2}) is 1.00 mm, while the length of the stubs (L) is 70.00 mm, and the length of the transmission line (L_t) is 15.74 mm. The gap between the input and output port is 0.4 mm, and the inner coupled stub gab is 0.2 mm. Open boundary conditions are applied to simulate the free-space behavior. Waveguide ports are defined at the input and output terminals to calculate the S_{11} parameter, allowing for

impedance matching analysis. The S_{11} parameter is a key performance indicator in RF and microwave system design. It measures the proportion of an incident signal that is reflected back toward the source due to impedance mismatch between the components. An S_{11} value of 0 dB denotes total reflection (i.e., complete mismatch), whereas values below -10 dB are typically considered indicative of acceptable matching, signifying that over 90% of the incident power is successfully transferred into the system.

To confirm the impedance matching characteristics of the proposed metamaterial transmission line, both the simulated and experimental results of the S_{11} parameter were examined. The fabricated metamaterial transmission line and the measurement setup of the S-parameter are shown in Figure 2 (b). The reflection coefficients of the proposed metamaterial transmission line structures were measured using a Keysight E5071C ENA Vector Network Analyzer, which was calibrated using the standard Short-Open-Load-Thru (SOLT) method.

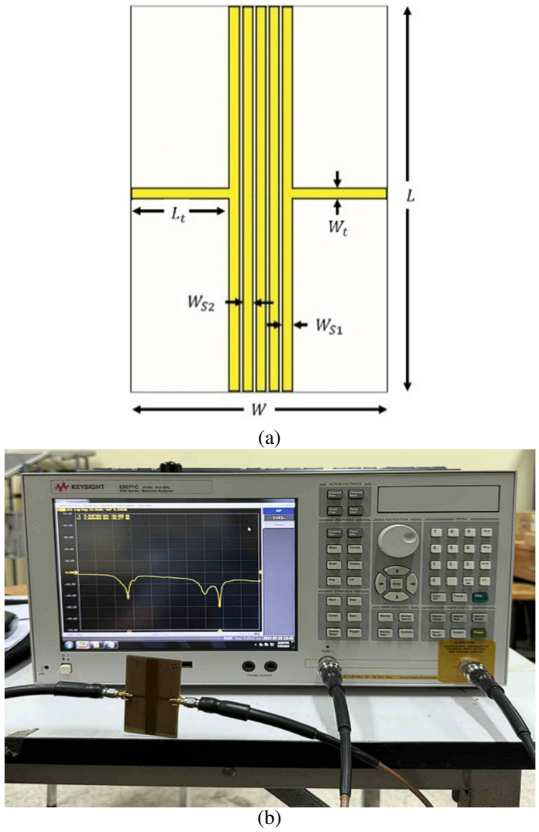

Fig. 2. (a) Geometry of the proposed metamaterial transmission line and (b) measurement setup.

A comparison of the reflection coefficient (S_{11}) between the simulated and measured results of the proposed metamaterial transmission line over the frequency range of 1.00 GHz to 6.00 GHz is displayed in Figure 3. The results show that both the simulation and measurement curves exhibit distinct resonant behaviors, marked by notable dips in the S_{11} values, indicating effective impedance matching and reduced signal reflection at these frequencies. Both the simulation and measurement results show the first frequency to be approximately 2.00 GHz-2.70 GHz with minimal dip values of -19.18 at 2.43 GHz and -23.32 at 2.40 GHz for the simulation and measurement results, respectively. The second band is from approximately 4.13 to 5.42 GHz with minimal dip values of -34.60 at 4.72 GHz and -28.27 at 5.03 GHz for the simulation and measurement results, respectively. These minima in the S_{11} trace confirm the existence of well-defined resonances and validate the effectiveness of the design in achieving multiband impedance matching. From the results, consistency appears in both the simulation and measurement, confirming the accuracy of the design and its physical realization. This strong agreement between the simulated and measured results confirms the accuracy of the design. The minor discrepancies observed are attributed to fabrication tolerances, which are common in practical implementations. Overall, these results demonstrate the effectiveness of the metamaterial transmission line in minimizing the reflection and optimizing the energy transfer across the targeted dual-band frequencies, as demonstrated in the experimental results of the energy harvesting performance in the next section.

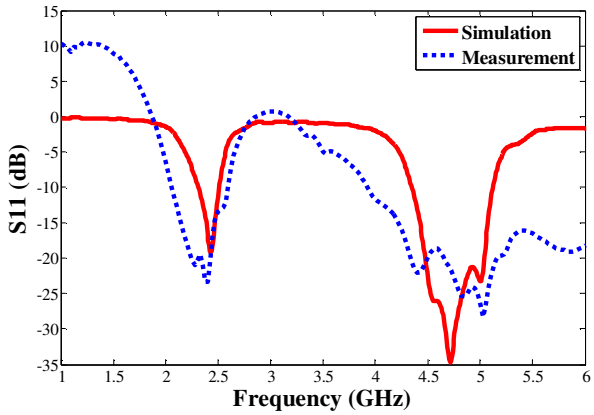

Fig. 3. Measured and simulated S_{11} parameters of metamaterial transmission line.

III. ENERGY HARVESTING TESTING

This section provides a comprehensive evaluation of the proposed metamaterial-based rectifier and rectenna system. Three test scenarios were considered, including rectifier efficiency testing, load-dependence performance and wireless energy harvesting rectenna response under varying transmission distances.

A. Measurements of Rectifier Efficiency

Following the S-parameter validation, which validates that the proposed metamaterial transmission line can achieve multiband impedance matching, the performance of the proposed metamaterial transmission line for the energy harvesting system was tested under laboratory conditions. In this phase, the system was connected in a manner consistent with Figure 1, although the receiving antenna was intentionally excluded from the setup. The RF signal was injected into the metamaterial transmission line, which directed the signal into

the rectification stage. The rectification circuit employed in the system was a half-wave rectifier utilizing an HSMS2860 Schottky diode, which was selected for its low threshold and high efficiency. The rectifier circuit also included a low-pass filter and a 1200 Ω resistive load. Figure 4 illustrates the measurement setup for the rectifier. It involved the utilization of the RF signal generator (Keysight N5172B EXG) as the source of the RF signal to transmit the signal into the metamaterial transmission line and rectifier. The input frequency was set to either 2.4 GHz and 5.0 GHz, and the input power level varied from -20 to +20 dBm.

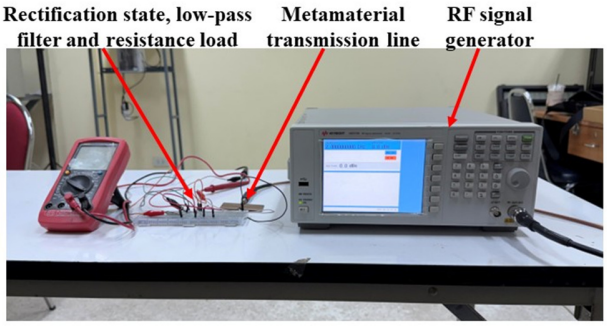

Fig. 4. Rectifier measurement setup.

First, the output voltage performance of the rectifier was measured to evaluate its practical DC output capability when used at frequencies of 2.4 and 5.0 GHz. Figure 5 depcts the measured output voltage (V_{out}) of a rectifier as a function of the input power (P_{in}) at two distinct frequency conditions at 2.40 GHz (f_L) and 5.00 GHz (f_H). The results show that at an input power below -10 dBm, the output voltage is low for both f_L and f_H because of insufficient activation of the rectifying diodes. As the amplitude of the input power increases, the output voltage rises sharply, reaching a nearly linear growth region between 0 dBm and 10 dBm. This indicates efficient rectification and optimal operation within this power window. The output voltage increases nearly linearly and reaches a saturation point at approximately 1.70 V and 1.66 V for f_L and f_H, respectively.

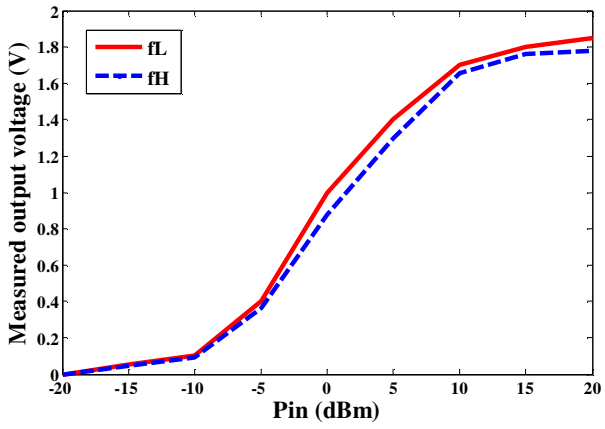

Fig. 5. Output voltage of the proposed rectifier.

Beyond this power input range, the voltage increase slows as the rectifier approaches saturation, likely due to non-ideal diode behavior and increased losses. Notably, the close agreement between the curves at f_L and f_H indicates a consistent voltage performance across the targeted frequency band. This confirms the frequency-insensitive nature of the design, which is critical for broadband RF energy harvesting systems.

To assess the power conversion capability of the rectifier, its RF-to-DC efficiency was measured as a function of the input power at two operating frequencies. This test revealed the optimal operating conditions and highlighted the dynamic response of the circuit at different power levels. For this test, the system was terminated with a fixed 1500 Ω resistor. The voltage drop across the load was measured using a digital multimeter and the efficiency was computed according to:

$$\eta = \left(\frac{V_{out}^2}{R_L.P_{in}}\right) \times 100\% \quad (1)$$

Figure 6 displays the RF-to-DC conversion efficiency of the proposed rectifier as a function of the input power (P_{in}) evaluated at two operating frequencies, denoted as f_L and f_H. The results demonstrated that the efficiency improved steadily with an increasing input power. It started from 10% at -20 dBm and reached a peak of approximately 72% at 5 dBm for f_L and 70% at 5 dBm for f_H. This behavior is characteristic of the nonlinear rectifying circuits, where optimal matching and diode turn-on conditions are achieved within a specific input power range. Beyond the peak point, the efficiency declined as P_{in} increased, and it decreased to 26% at 20 dBm for both frequencies. This is primarily due to diode saturation and increased conduction losses. The curves for f_L and f_H remained closely aligned throughout the input power sweep, demonstrating the rectifier's stable performance and broadband capability. The high efficiency achieved within the practical power range confirmed the suitability of the proposed rectifier for energy harvesting and wireless power transfer applications.

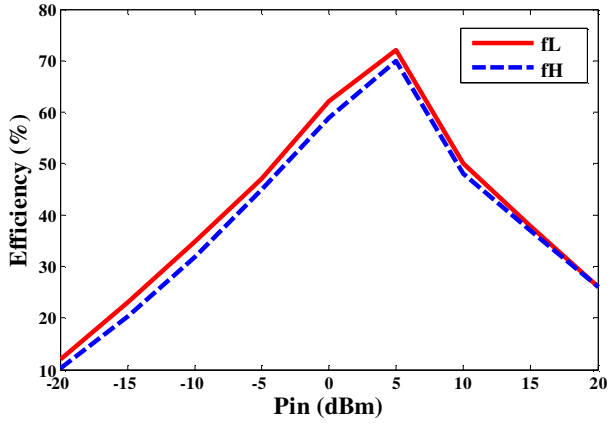

Fig. 6. Efficiency of the proposed rectifier.

B. Load-Dependent Performance

The final set of rectifier measurements explored the performance of the rectifier under different load conditions. The objective was to determine the optimal operating

conditions for maximizing the energy conversion. This analysis was critical for evaluating the circuit's adaptability in real-world scenarios, where the load resistance may not be fixed or well-controlled. The circuit was subjected to eight discrete load values of 1000 Ω, 1100 Ω, 1200 Ω, 1300 Ω, 1500 Ω, 1600 Ω, 1800 Ω, and 2000 Ω. The input frequency and power were held constant at 5 dBm during each load test and the efficiency was computed according to (1). Figure 7 presents a detailed analysis of the proposed system's efficiency as a function of input power under varying load resistances. The results are shown at two different operating frequencies: (a) the first band (f_L) and (b) the second band (f_H). The results show that across all configurations, the rectifier demonstrates a consistent trend of efficiency increases with increasing input power, peaks near 5 dBm, and subsequently declines owing to diode saturation and increased conduction losses.

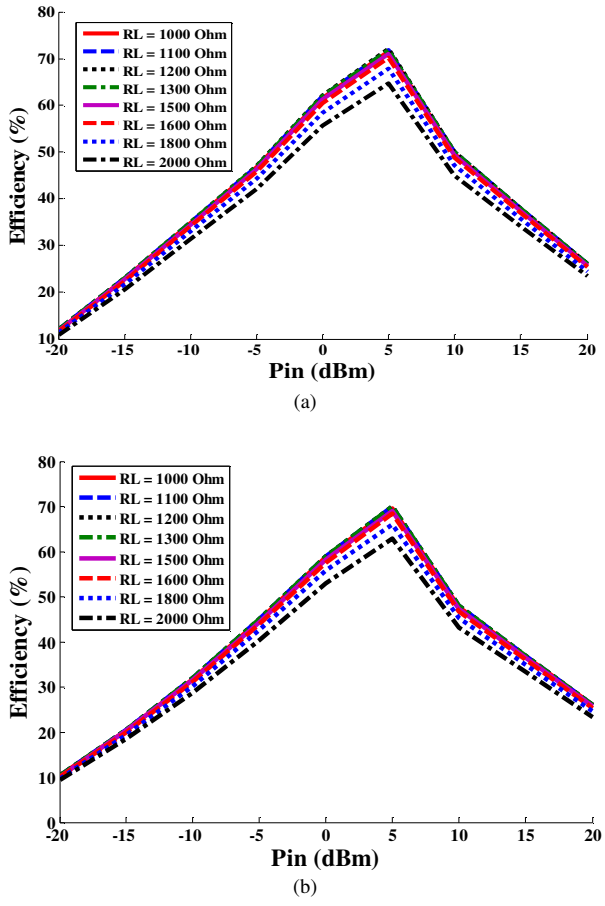

Fig. 7. The efficiency of the proposed rectifier under varying load resistances across different input power levels measured at two frequencies: (a) at first band (f_L) and (b) at second band (f_H).

At both frequencies, the optimal performance is observed for load resistances in the range of 1200 Ω –1600 Ω, where the peak efficiency exceeds 70%. This indicates the rectifier's sensitivity to load conditions and highlights the importance of proper load matching to maximize the energy conversion efficiency. For load values significantly above or below this optimal range, a gradual degradation in peak efficiency is evident, reflecting impedance mismatch and suboptimal power transfer. Overall, the rectifier exhibited stable behavior across a broad range of load conditions, maintaining an efficiency above 60% in most scenarios near the optimal input power region. These results confirm the robustness of the design and its applicability in environments where load variability is expected in energy harvesting systems.

The experimental findings provide valuable insights into the behavior of the proposed metamaterial-inspired transmission line when applied in RF energy harvesting systems as an impedance matching circuit part. The results confirmed that both the operating frequency and load resistance significantly affected the output voltage and conversion efficiency of the system. Overall, the proposed system demonstrated robust operation across a wide range of input powers and load conditions, with clear trade-offs between the voltage gain and efficiency depending on the frequency of operation. The lower-frequency configuration is more favorable for applications where the efficiency and energy conservation are critical, whereas the higher-frequency mode is better suited for scenarios requiring greater voltage output or sensitivity to weaker RF signals. These insights may guide future enhancements in adaptive impedance control and frequency-aware design to improve the versatility and overall energy harvesting capability of rectenna-based systems.

C. Measurement of Rectena Performance

As a final stage of evaluation, the complete rectenna system was tested to assess its wireless power reception capabilities. The objective of this test was to validate the system under realistic operating conditions. The rectenna was tested in a far-field setup to capture the RF energy transmitted through the free space. The measurement setup for the rectenna is illustrated in Figure 8, highlighting the integration of the antenna and rectification circuit to assess the overall efficiency of the energy harvesting system. A Wi-Fi access point (TP-Link Archer A6) was used to transmit 2.4 GHz and 5.0 GHz signals via dual 5 dBi monopole antennas. A standard horn antenna with an average gain of 8 dBm was used to capture the RF waves from the environment. This was tested/This was achieved by measuring the output voltage level generated at various distances from 0 to 250 cm. At each distance, the output voltage was recorded using a digital multimeter.

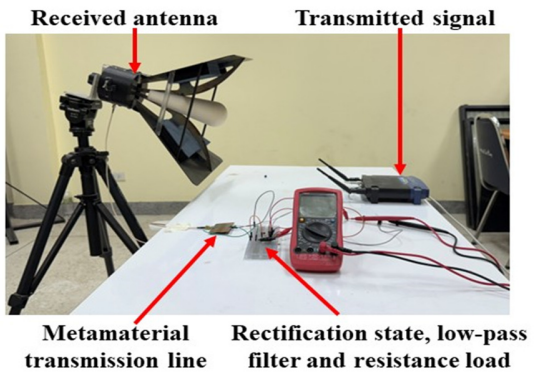

Fig. 8. Measurement of the rectenna setting.

Figure 9 shows the measured output voltage of the rectenna captured at 2.40 GHz, and 5.00 GHz from the transmission signal using the Wi-Fi access point, which is shown as a function of the distance between the transmitting antenna and receiving rectenna, ranging from 0 to 250 cm. The results show that the output voltage at distances from 0 to 50 cm is relatively stable at approximately 450 mV, and when the distance increases, the output voltage drops below 150 mV at 250 cm, reflecting the inverse-square law behavior typical of far-field wireless energy transfer. As expected, the output voltage exhibits a clear decreasing trend with increasing distance, primarily due to path loss and reduced incident RF power on the receiving antenna. Despite the reduction, the rectenna maintains a measurable output over extended distances, highlighting its effectiveness for low-power wireless energy harvesting in short- to mid-range applications.

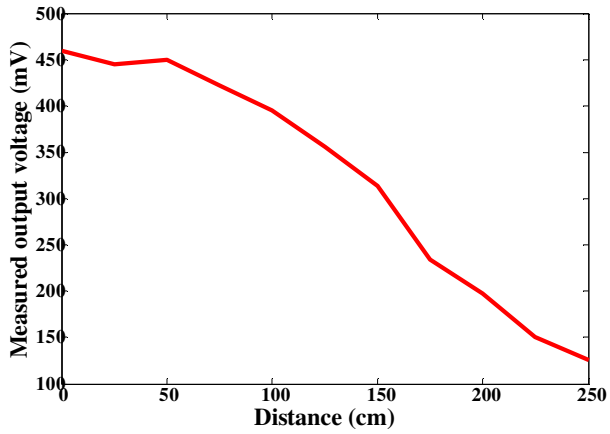

Fig. 9. Measured rectenna output voltage.

The comparative analysis in Table I emphasizes the impact of various impedance matching techniques on the system efficiency across different frequency bands. It has been demonstrated that traditional matching networks, including L-type circuits, stepped impedance stubs, and L-networks with short-circuited stubs, have been widely adopted due to their simplicity and established theoretical basis. These techniques are particularly effective for narrowband applications, where the circuit parameters can be precisely optimized for a single frequency. Among them, the stepped impedance stub method exhibits slightly superior performance, achieving up to 74% efficiency. However, these conventional approaches are typically less effective when extended to broadband or multiband systems. Their reliance on discrete components or fixed geometries often limit the adaptability and degrade their performance outside the design frequency.

Notably, a prior attempt at employing a metamaterial-based impedance matching network achieved only 8.8% efficiency when used with an RF-ambient, indicating substantial limitations in either the design methodology or material implementation. In contrast, the approach proposed in this work, which integrates metamaterial structures directly into the transmission line architecture, demonstrates markedly improved results, achieving peak efficiencies of 72% at 2.4 GHz and 70% at 5.0 GHz. The superior performance of the proposed configuration is largely attributed to the engineered electromagnetic characteristics of the metamaterials, which allow for precise impedance control and reduced signal reflection across a broader frequency range. Unlike conventional networks, which often require discrete components or complex geometries, the metamaterial transmission line offers a more compact and integrable solution.

TABLE I. COMPARATIVE ANALYSIS OF CONVENTIONAL AND METAMATERIAL-BASED MATCHING NETWORKS

Ref.	Operating frequency	Impedance matching technique	Peak efficiency
[26]	0.915 GHz and 2.45 GHz	L-type matching networks	71% and 67.7%
[27]	0.915 GHz and 2.45 GHz	Stepped impedance stub matching network	74% and 73%
[25]	1.80 GHz and 2.45 GHz	L-network with short-circuited shunt stub	72% and 65%
[24]	2.4 GHz and 5.0 GHz	Metamaterial impedance matching network	8.8%
This work	2.4 GHz and 5.0 GHz	Metamaterials transmission line matching network	72% and 70%

IV. CONCLUSIONS

This paper presents a dual-band Wi-Fi energy harvesting system based on the metamaterial transmission line technology. The proposed design demonstrated strong impedance matching characteristics, as confirmed through the reflection coefficient (S_{11}) analysis, and achieved reliable energy conversion performance over a wide range of input power levels and frequencies. The rectifier circuit delivered a peak Radio Frequency (RF)-to-DC efficiency of 72% and maintained a consistent output behavior across multiple load resistances, highlighting its robustness and versatility. Moreover, the distance-based rectenna testing confirmed the system's practical feasibility for far-field wireless energy collection, maintaining the output functionality at distances up to 250 cm. These findings confirm the potential of metamaterial-inspired transmission lines not only as effective impedance matching solutions, but also as a pathway toward miniaturized, broadband, and high-efficiency RF front-end systems suitable for next-generation wireless technologies. Furthermore, the proposed rectenna system offers a promising solution for powering low-power electronic devices in wireless sensor networks, ambient RF environments, and Internet of Things (IoT) platforms.

ACKNOWLEDGMENT

This research was financially supported by Mahasarakham University.

REFERENCES

[1] S. Salleh, M. A. Zakariya, and R. M. A. Lee, "A Comparison Study of Rectifier Designs for 2.45 GHz EM Energy Harvesting," *Energy and Power Engineering*, vol. 13, no. 2, pp. 81–89, Feb. 2021, https://doi.org/10.4236/epe.2021.132006.

[2] R. Sharma *et al.*, "Electrically connected spin-torque oscillators array for 2.4 GHz WiFi band transmission and energy harvesting," *Nature*

Communications, vol. 12, no. 1, May 2021, Art. no. 2924, https://doi.org/10.1038/s41467-021-23181-1.

[3] D. Pinto *et al.*, "Design and Performance Evaluation of a Wi-Fi Energy Harvester for Energizing Low Power Devices," in *2021 IEEE Region 10 Symposium (TENSYMP)*, Jeju, Republic of Korea, Aug. 2021, pp. 1–8, https://doi.org/10.1109/TENSYMP52854.2021.9551001.

[4] S. N. Deepa and B. S. S. Rani, "RF energy harvesting using 900MHz of mobile signal frequency to charging the mobile battery," in *2017 International Conference on Innovations in Green Energy and Healthcare Technologies (IGEHT)*, Coimbatore, India, Mar. 2017, pp. 1–5, https://doi.org/10.1109/IGEHT.2017.8094066.

[5] Mutee-Ur-Rehman, M. I. Qureshi, W. Ahmad, and W. T. Khan, "Radio frequency energy harvesting from ambient FM signals for making battery-less sensor nodes for wireless sensor networks," in *2017 IEEE Asia Pacific Microwave Conference (APMC)*, Kuala Lumpur, Malaysia, Nov. 2017, pp. 487–490, https://doi.org/10.1109/APMC.2017.8251487.

[6] P. Panmuang, A. Sonsilphong, and C. Soemphol, "RF-DC conversion for RF energy harvesting from digital TV signals using voltage multiplier circuits," *TELKOMNIKA (Telecommunication Computing Electronics and Control)*, vol. 22, no. 2, pp. 282–289, Apr. 2024, https://doi.org/10.12928/telkomnika.v22i2.25593.

[7] X. Liu, M. Li, X. Chen, Y. Zhao, L. Xiao, and Y. Zhang, "A Compact RF Energy Harvesting Wireless Sensor Node with an Energy Intensity Adaptive Management Algorithm," *Sensors*, vol. 23, no. 20, Jan. 2023, Art. no. 8641, https://doi.org/10.3390/s23208641.

[8] Y. Luo, L. Pu, G. Wang, and Y. Zhao, "RF Energy Harvesting Wireless Communications: RF Environment, Device Hardware and Practical Issues," *Sensors*, vol. 19, no. 13, Jan. 2019, Art. no. 3010, https://doi.org/10.3390/s19133010.

[9] T. D. T. Thanh, P. D. Quan, P. H. Phuc, and H. T. P. Thao, "A Penta-band Antenna using Symmetrical DGS for RF Energy Harvesting in IoT Applications," *Engineering, Technology & Applied Science Research*, vol. 15, no. 2, pp. 22028–22034, Apr. 2025, https://doi.org/10.48084/etasr.10138.

[10] M. Aboualalaa, I. Mansour, and R. K. Pokharel, "Energy Harvesting Rectenna Using High-Gain Triple-Band Antenna for Powering Internet-of-Things (IoT) Devices in a Smart Office," *IEEE Transactions on Instrumentation and Measurement*, vol. 72, pp. 1–12, 2023, https://doi.org/10.1109/TIM.2023.3238050.

[11] S. Roy, R. J.-J. Tiang, M. B. Roslee, Md. T. Ahmed, and M. A. P. Mahmud, "Quad-Band Multiport Rectenna for RF Energy Harvesting in Ambient Environment," *IEEE Access*, vol. 9, pp. 77464–77481, 2021, https://doi.org/10.1109/ACCESS.2021.3082914.

[12] J. Liu, M. Huang, and Z. Du, "Design of Compact Dual-Band RF Rectifiers for Wireless Power Transfer and Energy Harvesting," *IEEE Access*, vol. 8, pp. 184901–184908, 2020, https://doi.org/10.1109/ACCESS.2020.3029603.

[13] H. Sun, Y. Guo, M. He, and Z. Zhong, "A Dual-Band Rectenna Using Broadband Yagi Antenna Array for Ambient RF Power Harvesting," *IEEE Antennas and Wireless Propagation Letters*, vol. 12, pp. 918–921, 2013, https://doi.org/10.1109/LAWP.2013.2272873.

[14] J. Liu, X. Y. Zhang, and C.-L. Yang, "Analysis and Design of Dual-Band Rectifier Using Novel Matching Network," *IEEE Transactions on Circuits and Systems II: Express Briefs*, vol. 65, no. 4, pp. 431–435, Apr. 2018, https://doi.org/10.1109/TCSII.2017.2698464.

[15] Z. Liu, Z. Zhong, and Y.-X. Guo, "Enhanced Dual-Band Ambient RF Energy Harvesting With Ultra-Wide Power Range," *IEEE Microwave and Wireless Components Letters*, vol. 25, no. 9, pp. 630–632, Sep. 2015, https://doi.org/10.1109/LMWC.2015.2451397.

[16] M. Huang *et al.*, "Single- and Dual-Band RF Rectifiers with Extended Input Power Range Using Automatic Impedance Transforming," *IEEE Transactions on Microwave Theory and Techniques*, vol. 67, no. 5, pp. 1974–1984, May 2019, https://doi.org/10.1109/TMTT.2019.2901443.

[17] C.-H. Li, M.-C. Yu, and H.-J. Lin, "A Compact 0.9-/2.6-GHz Dual-Band RF Energy Harvester Using SiP Technique," *IEEE Microwave and Wireless Components Letters*, vol. 27, no. 7, pp. 666–668, Jul. 2017, https://doi.org/10.1109/LMWC.2017.2711506.

[18] K. Niotaki, A. Georgiadis, A. Collado, and J. S. Vardakas, "Dual-Band Resistance Compression Networks for Improved Rectifier Performance," *IEEE Transactions on Microwave Theory and Techniques*, vol. 62, no. 12, pp. 3512–3521, Dec. 2014, https://doi.org/10.1109/TMTT.2014.2364830.

[19] J. B. Pendry, A. J. Holden, D. J. Robbins, and W. J. Stewart, "Magnetism from conductors and enhanced nonlinear phenomena," *IEEE Transactions on Microwave Theory and Techniques*, vol. 47, no. 11, pp. 2075–2084, Nov. 1999, https://doi.org/10.1109/22.798002.

[20] C. Soemphol, S. F. Kitchin, M. A. Fiddy, and N. Wongkasem, "Electromagnetic responses of curved fishnet structures: near-zero refractive index with lower loss," *Journal of Optics*, vol. 18, no. 2, Dec. 2015, Art. no. 025102, https://doi.org/10.1088/2040-8978/18/2/025102.

[21] A. Rennings, S. Otto, T. Liebig, C. Caloz, and I. Wolff, "Extended composite right/left-handed (E-CRLH) metamaterial and its application as quadband quarter-wavelength transmission line," presented at the Asia-Pacific Microwave Conference (APMC 2006), Yokohama, Japan, 2006, pp. 1405–1408, https://doi.org/10.1109/apmc.2006.4429669.

[22] C. Damm, M. Schussler, J. Freese, and R. Jakoby, "Novel impedance matching approach employing the band gap region of composite right/left-handed artificial lines," in *2007 European Microwave Conference*, Munich, Germany, Oct. 2007, pp. 708–711, https://doi.org/10.1109/EUMC.2007.4405290.

[23] F. Paredes, G. Zamora, J. Bonache, and F. Martín, "Perturbation method based on resonant type metamaterial transmission lines for dual-band matching networks," in *2009 Mediterrannean Microwave Symposium (MMS)*, Tangiers, Morocco, Nov. 2009, pp. 1–4, https://doi.org/10.1109/MMS.2009.5409764.

[24] E. Coskuner and J. J. Garcia-Garcia, "Metamaterial Impedance Matching Network for Ambient RF-Energy Harvesting Operating at 2.4 GHz and 5 GHz," *Electronics*, vol. 10, no. 10, Jan. 2021, Art. no. 1196, https://doi.org/10.3390/electronics10101196.

[25] R. Maher, A. Allam, H. Kanaya, and A. B. Abdelrahman, "Dualband rectenna for RF energy harvesting using metamaterial reflect array and novel matching technique," *AEU - International Journal of Electronics and Communications*, vol. 173, Jan. 2024, Art. no. 155020, https://doi.org/10.1016/j.aeue.2023.155020.

[26] D. Lee and J. Oh, "Broad Dual-Band Rectifier With Wide Input Power Ranges for Wireless Power Transfer and Energy Harvesting," *IEEE Microwave and Wireless Components Letters*, vol. 32, no. 6, pp. 599–602, Jun. 2022, https://doi.org/10.1109/LMWC.2022.3145879.

[27] S. Li, F. Cheng, C. Gu, S. Yu, and K. Huang, "Efficient Dual-Band Rectifier Using Stepped Impedance Stub Matching Network for Wireless Energy Harvesting," *IEEE Microwave and Wireless Components Letters*, vol. 31, no. 7, pp. 921–924, Jul. 2021, https://doi.org/10.1109/LMWC.2021.3078546.